ADVANCES IN ATMOSPHERIC SCIENCES, VOL. 39, JULY 2022, 1021–1033

• **Original Paper** •

Intensity Evolution of Zonal Shear Line over the Tibetan Plateau in Summer: A Perspective of Divergent and Rotational Kinetic Energies※

Xiaohong BAO[1,2] and Xiuping YAO[*2,1]

[1]*State Key Laboratory on Severe Weather*, *Chinese Academy of Meteorological Sciences*, *Beijing* 100081, *China*
[2]*China Meteorological Administration Training Centre*, *Beijing* 100081, *China*

(Received 13 August 2021; revised 15 November 2021; accepted 2 December 2021)

ABSTRACT

Based on the ERA5 reanalysis datasets during 1980–2019, a total of eleven zonal shear lines (ZSLs) that caused heavy precipitation and lasted more than 60 hours over the Tibetan Plateau in summer are selected for composite analysis. By decomposing the kinetic energy (K) near the ZSL into divergent and rotational kinetic energies (K_D and K_R) and the kinetic energy of interaction between the divergent wind and the rotational wind (K_{RD}), the influence of the rotational and divergent winds on the evolution of the ZSL intensity is investigated from the perspective of K_D and K_R. The main results are as follows. The ZSL is a comprehensive reflection of rotation and convergence. The intensity evolution of ZSL is essentially synchronized with those of K, K_R, and K_{RD} but lags behind K_D by about three hours. The enhancement of K is mainly contributed by K_R, which is governed by the conversion from K_D to K_R. Furthermore, the increase in the conversion from K_D to K_R is controlled by the geostrophic effect term Af, which is determined by the joint enhancement of the zonal rotational and meridional divergent wind components (u_R and v_D). Therefore, the joint enhancement of u_R and v_D controls the increase of the ZSL intensity, leading to increased precipitation.

Key words: zonal shear line over the Tibetan Plateau, intensity evolution, divergent and rotational kinetic energies, joint action of the zonal rotational and meridional divergent wind components

Citation: Bao, X. H., and X. P. Yao, 2022: Intensity evolution of zonal shear line over the Tibetan Plateau in summer: A perspective of divergent and rotational kinetic energies. *Adv. Atmos. Sci.*, **39**(7), 1021−1033, https://doi.org/10.1007/s00376-021-1302-9.

Article Highlights:

- The intensity evolution of ZSL is basically synchronized with those of K and K_R but lags behind K_D by about three hours.
- The enhancement of K is mainly contributed by that of K_R, which is governed by the conversion from K_D to K_R.
- The joint enhancement of u_R and v_D intensifies the conversion from K_D to K_R and helps increase the ZSL intensity.

1. Introduction

As a plateau with the highest elevation in the world and the largest area in the Northern Hemisphere, the Tibetan Plateau (TP) has an average elevation of more than 4000 m and accounts for one-quarter of China's land area. It has unique weather and climate characteristics that significantly affect the atmospheric circulation, weather, and climate in China, Asia, and globally. Therefore, TP meteorology, which focuses on its dynamic and thermal forcing, was recognized early by researchers and has since become an important research field in weather and climate (Bolin, 1950; Flohn, 1957; Wu et al., 2004).

Under the unique dynamic and thermal effects of the TP, two types of typical cyclonic circulation systems with low–geopotential-height structures are isolated and named the plateau shear line and the plateau vortex. Both are formed in the near-surface layer over the TP. Research has shown that the occurrence frequency of plateau shear lines and the frequency of shear line-induced precipitation are greater than those of plateau vortexes (The Tibetan Plateau Science Research Group, 1981; He et al., 2009). Furthermore, the plateau shear lines can be categorized into the zonal shear lines with a quasi-east-west orientation and the meridional shear lines with a quasi-south-north orientation. Comparatively, zonal shear lines occur more often and have a longer duration; moreover, they experience greater difficulty to propagating out of the TP and thereby more likely to cause potential disastrous heavy precipitation over the TP

※ This paper is a contribution to the special issue on Third Pole Atmospheric Physics, Chemistry, and Hydrology.

* Corresponding author: Xiuping YAO
Email: yaoxp@cma.gov.cn

(Ye and Gao, 1979; Tao et al., 1984; Zhang et al., 2016; Zhang et al., 2019; Yao et al., 2020). Statistics have shown that during the boreal summer half-year over the TP, more than 50% of zonal shear lines caused heavy precipitation, and about 40% of heavy precipitation days are related to zonal shear lines (Zhang et al., 2016). Therefore, the zonal shear line (ZSL) over the TP in summer is one of the essential factors accounting for the occurrence of disastrous weather over the TP (Note: ZSL mentioned in this research all refers to ZSL over the TP in summer), and the study on the ZSL evolution is of great significance to the forecasting and early-warning of disastrous weather.

Key to this complex research, it is generally accepted that the evolution of ZSLs is mainly driven by the dynamic and thermal effects of the TP (The Tibetan Plateau Science Research Group, 1981; Ye, 1981; Tao, 1980) and is subject to large-scale circulation systems such as the western Pacific subtropical high (The Tibetan Plateau Science Research Group, 1981), the Iran high (Tang, 2002) and the South Asia high (Shi and He, 2011). Many diagnostic analyses on ZSL evolution have been carried out. The results show that the formation, development, and maintenance of the ZSL are closely associated with the development of various factors, including the large-scale ascending motion at 500 hPa (Yu, 1994), the local vorticity center or vorticity zone (Tu and He, 2010), the generalized moist potential vorticity center (Chen and Li, 2018), the apparent heat source and apparent moisture sink (Zhao and Yao, 2018), etc. In addition, some scholars have obtained significant results from the perspective of kinetic energy for individual cases. For example, the main energy source during the processes of ZSL evolution is the transformation from available potential energy into kinetic energy (Yu and Luo, 1993). The conversion from eddy available potential energy to eddy kinetic energy (Luo and Li, 2019a) and the downscaled energy cascade of kinetic energy caused by the interaction between the background circulation and eddy field are conducive to the formation and development of ZSLs (Luo and Li, 2019b).

The ZSL is a discontinuous line in the cyclonic rotational wind field in the near-surface layer over the TP (Tao, 1980), featured by mid-tropospheric cyclonic rotation and horizontal wind field convergence. In addition, both the convergence (Fu et al., 2011; Zhou et al., 2014) and the rotation (Zhao et al., 2009; Fu et al., 2013; Li et al., 2019; Jin et al., 2020) of the wind field play essential roles in the development of weather systems. So, what are the respective effects of the divergent and rotational winds on the evolution of ZSLs? Research into this problem will help further promote the understanding of why ZSLs evolve. However, it is difficult to study the ZSL evolution using only the rotational and divergent winds by themselves. It is well known that kinetic energy plays a vital role in the evolution of weather systems and is directly related to the wind field. Therefore, it is helpful to study the problem mentioned above from the perspective of kinetic energy.

According to the Helmholtz theorem, the horizontal velocity can be uniquely decomposed into the rotational and divergent winds (Hawkins and Rosenthal, 1965), and correspondingly, the kinetic energy can be decomposed, in a similar manner, into its divergent and rotational kinetic energies and the kinetic energy of interaction between the divergent wind and the rotational wind. On this basis, numerous investigations have been conducted on weather systems from the perspective of divergent and rotational kinetic energies, such as tropical cyclones (Ding and Liu, 1986; Yu et al., 1999a, b; Zhao et al., 2009), extratropical cyclones (Pearce, 1974; Chen et al., 1978; Li et al., 2019; Jin et al., 2020), mesoscale convective complexes in North America (Fuelberg and Browning, 1983; Buechler and Fuelberg, 1986), circulation systems during the mei-yu periods (Fu et al., 2013) and the northeast cold vortex (Deng et al., 2012). The results revealed that the enhancement of weather systems is mainly caused by the increase in the rotational kinetic energy in the lower troposphere (Zhao et al., 2009; Fu et al., 2013; Li et al., 2019; Jin et al., 2020). Although the divergent kinetic energy is usually less than 10% of the kinetic energy (Pearce,1974; Ding and Liu, 1986), it is critical to the generation and conversion of kinetic energy (Fuelberg and Browning, 1983; Buechler and Fuelberg, 1986). However, there is no precedent to investigate the ZSL evolution through the perspective of divergent and rotational kinetic energies, although great achievements have been made in studying the evolution of many other weather systems through this theorem.

Therefore, it is of great significance to study the influence of the rotational and divergent winds on the evolution of the ZSL intensity from the perspective of the rotational and divergent kinetic energies, which provides a new point of view and insight for the in-depth understanding of the ZSL evolution.

The remainder of this paper is organized as follows. Section 2 introduces the data and methods. Section 3 provides the relationship of the ZSL intensity evolution with the rotational and divergent kinetic energies. Section 4 illustrates the mechanisms for the ZSL intensity evolution. Finally, section 5 presents the main conclusions and final discussion.

2. Data and Methods

2.1. *Data*

The data adopted in this study includes two datasets (1) the hourly wind dataset with a horizontal resolution of 1°×1° from June to August during 1980–2019 derived from the ERA5 reanalysis dataset and (2) the daily precipitation data (1200 UTC–1200 UTC) over the same period from the daily dataset of basic meteorological elements of China's National Surface Weather Station (version 3.0) released by the National Meteorological Information Centre of China Meteorological Administration.

2.2. *Methods*

2.2.1. *Case selecting for composite analysis of ZSLs*

Based on the wind data from the ERA5 reanalysis data-

set at 500 hPa from June to August during 1980–2019, the ZSLs are identified by an objective method with three parameters: the zonal shear of the meridional wind, the relative vorticity, and the zero line of meridional wind (Ma and Yao, 2015; Zhang et al., 2016). The specific criteria are as follows.

$$\begin{cases} \dfrac{\partial u}{\partial y} < 0 \\ \zeta > 0 \\ u = 0 \end{cases}, \tag{1}$$

where u is the zonal wind component, y indicates the meridional coordinate, ζ is the vertical component of the relative vorticity. When the three criteria in Eq. (1) are met at each grid point, the line connecting these grids, with a zonal span of more than 5 degrees of longitude, is identified as a ZSL.

Subsequently, in the high-frequency area of ZSLs (32°–35°N), which is located in a region with an altitude of more than 3000 m over the TP, the ZSLs with a lifetime longer than 24 hours are selected to form a dataset of ZSL cases. Furthermore, based on the daily precipitation data mentioned above, the ZSL case that causes heavy precipitation is defined by following these steps:

(1) The precipitation averaged at all stations on a certain day near each ZSL case (30°–36°N) in the dataset is defined as the average precipitation of that day (x_i, i=1, n. n indicates the total ZSL days in the dataset).

(2) The average daily precipitation for all cases and their standard deviation are expressed as:

$$\bar{x} = \frac{1}{n}\sum_{i=1}^{n} x_i \text{ and } \sigma = \sqrt{\frac{1}{n}\sum_{i=1}^{n}(x_i - \bar{x})^2}. \tag{2}$$

(3) If the x_i in a certain ZSL at any time over the course of its lifetime is one σ greater than $\bar{x}$, then this case is defined as a ZSL case that caused heavy precipitation.

Consequently, 11 typical cases that caused heavy precipitation and have a similar lifetime of more than 60 hours are selected from the above cases (Table 1). The distribution of the lifetime-averaged ZSLs from the 11 cases is shown in Fig. 1a.

Finally, the arithmetic average method is performed on each physical quantity of all typical cases at individual moments, with the intent of obtaining a composite ZSL for subsequent diagnostic analysis. The composite ZSL has a life-

Table 1. Elevent typical cases of zonal shear lines (ZSLs) over the Tibetan Plateau (TP) in summer (Note: ZSL mentioned in this research all refers to ZSL over the TP in summer. The avereage precipitation at all stations of each ZSL process near each ZSL case (30°–36°N) is defined as the accumulated precipitation. The LST represents the local solar time, which is six hours ahead of the coordinated universal time (UTC), that is, LST = UTC + 6 h, the same below.).

Serial number	Starting time (LST)	Ending time (LST)	Lifetime (h)	Accumulated precipitation (mm)
1	1980070516	1980070807	64	15.94
2	1982062417	1982062705	61	22.42
3	1983062615	1983062912	70	24.52
4	1985060715	1985061006	64	16.39
5	1985082114	1985082410	69	28.87
6	1987070816	1987071109	66	24.08
7	1991080414	1991080710	69	17.92
8	1992062217	1992062514	70	21.85
9	1992062517	1992062810	66	25.06
10	1996072314	1996072604	63	17.85
11	2018061118	2018061412	67	17.82

Note: For example, 2018061118 refers to 1800 LST 11 June 2018.

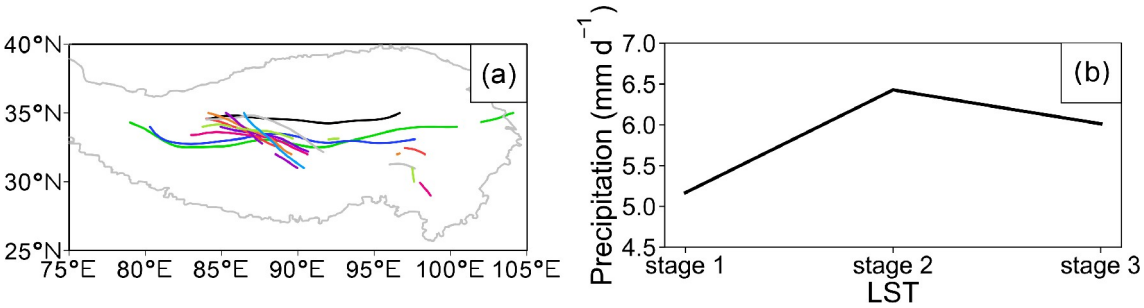

Fig. 1. (a) The distribution of 11 typical cases of lifetime-averaged ZSLs at 500 hPa (color contours), (b) The synthetic precipitation near the ZSL during its whole lifetime, the three stages, namely 1800 LST 1st–1800 LST 2nd, 1800 LST 2nd –1800 LST 3rd, and 1800 LST 3rd –1800 LST 4th (units: mm d^{-1}). The solid gray line outlines the region with an altitude of 3000 m, which indicates the major body of the TP (the same below).

time of 72 hours (1300 LST 1st–1200 LST 4th, short for 1300 LST on the 1st day to 1200 LST on the 4th day, the same below). Here, the LST represents the local solar time, six hours ahead of the coordinated universal time (UTC), LST = UTC + 6 h. It is important to note that the ZSL mentioned in the section below all refer to the composite ZSL from the 11 typical cases.

Given that the starting time of the ZSL is close to the starting time of the 24-hour accumulated precipitation, the precipitation near the ZSL during its whole lifetime is represented by the precipitation of the three stages, namely 1800 LST 1st–1800 LST 2nd, 1800 LST 2nd –1800 LST 3rd, and 1800 LST 3rd –1800 LST 4th (Fig. 1b).

2.2.2. *Stages of intensity evolution processes of ZSL*

The arithmetic average method is performed on the ZSL over the course of its lifetime. Considering the high-frequency region for the ZSL's occurrence (Zhang et al., 2016) and the large-value region of the ζ (greater than 2×10^{-5} s^{-1}), the region of 32°–35°N, 81°–99°E is selected as the study area, as shown in the red dashed box in Fig. 2a. The ZSL represents a unique weather system in the boundary layer over the TP, generally referring to a 500-hPa convergence line with opposite wind directions at more than three stations (The Tibetan Plateau Science Research Group, 1981). Therefore, the ZSL intensity is expressed by the regional-averaged ζ in the study area at 500 hPa. According to the ZSL intensity evolution (Fig. 4), the evolutionary processes are divided into the development stage (1300 LST 1st–1200 LST 2nd), the vigorous stage (1300 LST 2nd –1200 LST 3rd), and the decay stage (1300 LST 3rd –1200 LST 4th). The mean values of the physical quantities at each stage represent the environment of the ZSL evolution at each stage. There is an enhancement of the ZSL from the development stage to the vigorous stage and a weakening from the vigorous stage to the decay stage. The evolution of ZSL intensity is essentially synchronized with that of precipitation related to the ZSL (Fig. 1b). Note that the thermal effects of the TP exhibit significant diurnal variations, but this is not the focus of this study. To remove the influence of the diurnal variation on the ZSL evolution, the same start and end times are set for each stage to maintain consistency regarding the effect of diurnal variations.

2.2.3. *Divergent and rotational kinetic energies*

Based on the hourly wind dataset mentioned above, an iterative method (Endlich, 1967) with high computational efficiency and high accuracy is used to decompose the original horizontal wind ($\boldsymbol{V}$) into the rotational wind ($\boldsymbol{V}_R$) and the divergent wind ($\boldsymbol{V}_R$):

$$\boldsymbol{V} = \boldsymbol{V}_R + \boldsymbol{V}_D \,. \tag{3}$$

The bias for the divergence at each grid is less than or equal to 1×10^{-8} s^{-1} during the iterative process, which is less than or equal to 0.1% of the maximum divergence of the original horizontal wind field. The formulas for divergent and rotational kinetic energies are as follows.

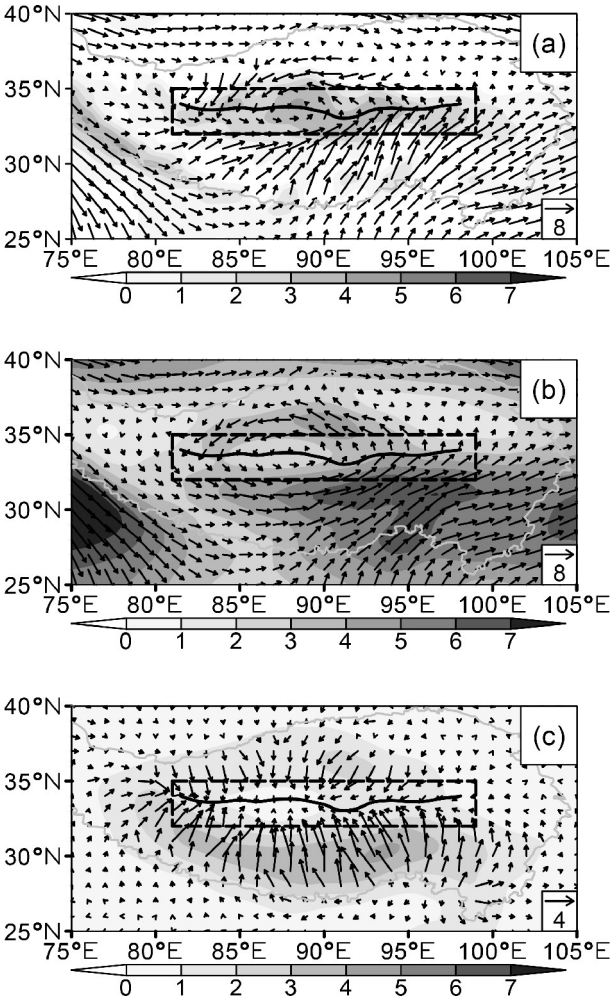

Fig. 2. (a) 500-hPa wind field (V) (black wind vectors; units: m s^{-1}) and the vertical component of the relative vorticity (ζ) (>0, shading; units: 10^{-5} s^{-1}), (b) 500-hPa rotational wind (V_R) and its specific value (black wind vectors and shading; units: m s^{-1}) and (c) 500-hPa convergent wind (V_R) and its specific value (black wind vectors and shading; units: m s^{-1}) averaged in the whole lifetime of the ZSL. The black dashed box represents the study area (32°–35°N, 81°–99°E), and the black thick solid line denotes the lifetime-averaged ZSL (the same below).

The kinetic energy per unit mass is expressed as:

$$k = \frac{1}{2}\boldsymbol{V}\cdot\boldsymbol{V} = k_R + k_D + \boldsymbol{V}_R\cdot\boldsymbol{V}_D \,, \tag{4}$$

where

$$k_D = \frac{1}{2}\boldsymbol{V}_D\cdot\boldsymbol{V}_D \text{ and } k_R = \frac{1}{2}\boldsymbol{V}_R\cdot\boldsymbol{V}_R \,. \tag{5}$$

The kinetic energy of an atmospheric volume in isobaric coordinates (A is the horizontal computational area) is given by:

$$K = K_D + K_R + \iint \boldsymbol{V}_R\cdot\boldsymbol{V}_D = K_D + K_R + K_{RD} \,, \tag{6}$$

where

$$K = \iint k, K_{\mathrm{D}} = \iint k_{\mathrm{D}}, K_{\mathrm{R}} = \iint k_{\mathrm{R}},$$
$$K_{\mathrm{RD}} = \iint \boldsymbol{V}_{\mathrm{R}} \cdot \boldsymbol{V}_{\mathrm{D}} \text{ and } \iint = \frac{1}{gA} \iint \mathrm{d}x\mathrm{d}y\mathrm{d}p\,. \quad (7)$$

K is the kinetic energy in a limited area (hereafter referred to as kinetic energy), K_{R} is the rotational kinetic energy, K_{D} the divergent kinetic energy, and K_{RD} is the kinetic energy of the interaction between the divergent wind and the rotational wind. Note that the sign of K_{RD} depends on the divergent and rotational wind directions.

The equation for rotational kinetic energy (Buechler and Fuelberg, 1986) is expressed as follows.

$$\underset{\mathrm{DK_R}}{\frac{\partial K_{\mathrm{R}}}{\partial t}} = \underset{I_{\mathrm{R}}}{\iint -\boldsymbol{V}_{\mathrm{R}} \cdot \frac{\partial \boldsymbol{V}_{\mathrm{D}}}{\partial t}} + \underset{\mathrm{Af}}{\iint -f(v_{\mathrm{R}}u_{\mathrm{D}} - u_{\mathrm{R}}v_{\mathrm{D}})} + \underset{\mathrm{Az}}{\iint -\zeta(v_R u_D - u_R v_D)} + \underset{B}{\iint -\omega \frac{\partial k_{\mathrm{R}}}{\partial p}} + \underset{C}{\iint -\omega \boldsymbol{V}_{\mathrm{R}} \cdot \frac{\partial \boldsymbol{V}_{\mathrm{D}}}{\partial p}}$$
$$+ \underset{G_{\mathrm{R}}}{\iint -\boldsymbol{V}_{\mathrm{R}} \cdot \nabla\phi} + \underset{\mathrm{HF_R}}{\iint -\nabla \cdot k\boldsymbol{V}_{\mathrm{R}}} + \underset{F_{\mathrm{R}}}{\iint -\boldsymbol{V}_{\mathrm{R}} \cdot \boldsymbol{F}}\,. \quad (8)$$

Here, u_{R} and u_{D} are the zonal rotational and divergent wind components, v_{R} and v_{D} are the meridional rotational and divergent wind components, ω is the vertical velocity (Pa s^{-1}), f is the Coriolis parameter, φ is the geopotential, and $\boldsymbol{F}$ is the frictional force.

For Eq. (8), the sum of Af, Az, B, and C is hereafter denoted as $C(K_{\mathrm{D}}, K_{\mathrm{R}})$. Therefore, Eq. (8) can be simplified as $\mathrm{DK_R} = I_{\mathrm{R}} + C(K_{\mathrm{D}}, K_{\mathrm{R}}) + G_{\mathrm{R}} + \mathrm{HF_R} + F_{\mathrm{R}}$. The term on the left-hand side, $\mathrm{DK_R}$, is the change term of K_{R} and denotes the local change of K_{R}. The term I_{R} is the change of K_{R} caused by the nonlinear interaction between the rotational wind and divergent wind. The term $C(K_{\mathrm{D}}, K_{\mathrm{R}})$ is a conversion term between K_{D} and K_{R}, including four terms of Af, Az, B, and C, a $C(K_{\mathrm{D}}, K_{\mathrm{R}})$ greater than zero indicates a conversion from K_{D} to K_{R}. The term Af is the geostrophic effect term. Both terms Af and Az are affected by relative orientations and magnitudes of $\boldsymbol{V}_{\mathrm{R}}$ and $\boldsymbol{V}_{\mathrm{D}}$. Term B describes the vertical exchange of K_{R}, while term C is related to the configuration of $\boldsymbol{V}_{\mathrm{D}}$ with $\boldsymbol{V}_{\mathrm{D}}$ and the vertical distribution of $\boldsymbol{V}_{\mathrm{D}}$. Term G_{R} is the generation term for K_{R}, indicating the conversion between K_{R} and the available potential energy due to the cross-contour flow of $\boldsymbol{V}_{\mathrm{R}}$. The term $\mathrm{HF_R}$ denotes the horizontal flux divergence of K by $\boldsymbol{V}_{\mathrm{R}}$. The term $\mathrm{F_R}$ represents friction and is related to the rotational wind, denoting frictional processes and the energy transfer between resolvable and unresolvable scales of motion. As it is calculated as the residual, possible errors from other terms are also included in Eq. (8).

3. Relationship of the ZSL intensity evolution with the divergent and rotational kinetic energies

Previous studies have revealed that the ZSL is mainly located below 400 hPa (Tao, 1984), indicating a relatively shallow system. Therefore, this study mainly targets levels below 400 hPa.

3.1. *Distribution Characteristics of the divergent and rotational winds*

Figures 2b-c illustrate that $\boldsymbol{V}$ at 500 hPa is well-decomposed into $\boldsymbol{V}_{\mathrm{R}}$ and $\boldsymbol{V}_{\mathrm{D}}$. The magnitude and distribution of $\boldsymbol{V}_{\mathrm{R}}$ are similar to those of $\boldsymbol{V}$, while the magnitude of $\boldsymbol{V}_{\mathrm{D}}$ is obviously smaller than that of $\boldsymbol{V}$ (Fig. 2a). Moreover, the wind speeds of $\boldsymbol{V}_{\mathrm{R}}$ and $\boldsymbol{V}_{\mathrm{D}}$ tend to be small near the ZSL but are larger on the north and south sides, in the vicinity of ZSL, especially on the south side. A cyclonic circulation of $\boldsymbol{V}_{\mathrm{R}}$ and the convergence of $\boldsymbol{V}_{\mathrm{D}}$ appears near the ZSL. In addition, the circulation center of $\boldsymbol{V}_{\mathrm{R}}$ is located on the ZSL, but the strongest convergence appears on the south side of the ZSL.

In summary, there are cyclonic $\boldsymbol{V}_{\mathrm{R}}$ and convergent $\boldsymbol{V}_{\mathrm{D}}$ near the ZSL, and the magnitude of $\boldsymbol{V}_{\mathrm{R}}$ is larger than that of $\boldsymbol{V}_{\mathrm{D}}$.

3.2. *Spatial evolution characteristics of the kinetic energy and its components*

Figure 3 shows that during the entire lifetime of the ZSL at 500 hPa, K, K_{R}, K_{D}, the absolute value of K_{RD} are smaller near the ZSL but larger on its north and south sides, especially in the southeast quadrant of the ZSL. The distribution characteristics of these physical quantities depend on the distribution of the horizontal wind field, as shown in Fig. 2. Specifically, there is a dense zone of K contours in the southeast quadrant of the study area at the development stage, and the maximum K reaches 25 J m^{-2} at this stage (Fig. 3a). In the vigorous stage (Fig. 3b), K increases throughout the entire study area, and the maximum value increases to 35 J m^{-2}. In addition, the increase in the gradient of K in the southeast quadrant of the study area is especially significant. Figure 3c shows that K decreases throughout the entire study area in the decay stage, noting that the gradient of K in the southeast quadrant decreases significantly, with the maximum K dropping down to 30 J m^{-2}. The change of gradient of K near the ZSL is basically consistent with the ZSL intensity evolution, which agrees with the results in Luo and Li (2019a). The evolution of K_{R} (Figs. 3a1–c1) and K_{D} (Figs. 3a2–c2) near the ZSL are similar to that of K but numerically smaller. The K_{RD} shows uneven distributions (Figs. 3a3–c3), with positive (negative) values in the western (eastern) part of the study area, but its absolute values also increase (decrease) with the development (decay) of the ZSL. The evolution trend of the kinetic energy and its components in the vertical direction is sim-

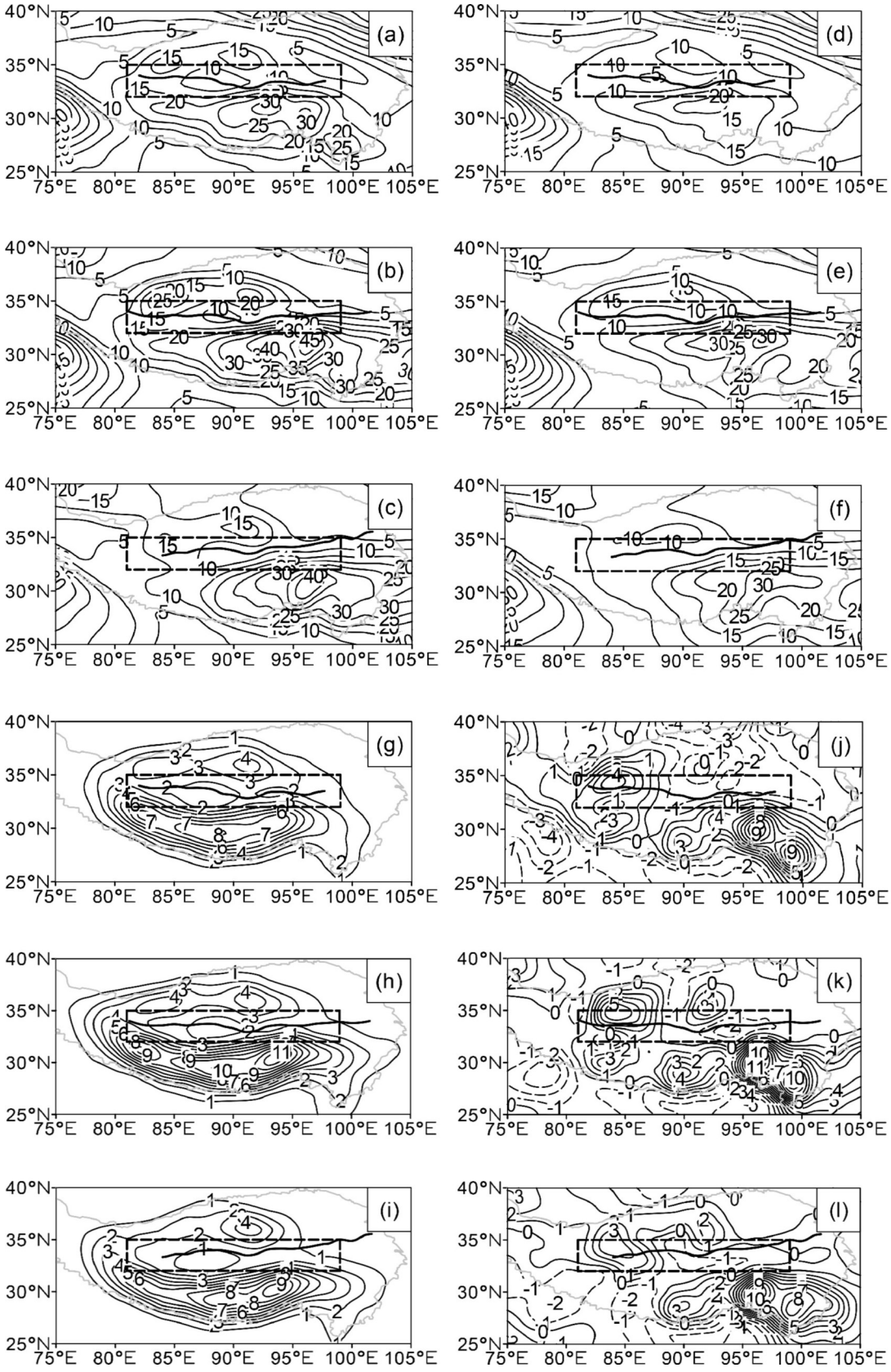

Fig. 3. (a–c) The kinetic energy (K), (d–f) the rotational kinetic energy (K_R), (g–i) the divergent kinetic energy (K_D), and (j–l) the kinetic energy for the interaction between the divergent wind and the rotational wind (K_{RD}) at 500 hPa (contours, units: J m^{-2}) averaged at different stages of the ZSL. (a, d, g, j) denote the development stage, (b, e, h, k) the vigorous stage, and (c, f, i, l) the decay stage.

ilar to that in the horizontal direction (figure omitted).

3.3. *Response of the kinetic energy and its components to the evolution of the ZSL intensity*

The above analysis is based on the mean ZSL averaged at each stage, through which how much time the response of K and its components (K_R, K_D, K_{RD}) to the evolution of the ZSL intensity takes cannot be determined. As mentioned above, the 500 hPa relative vorticity ζ represents the ZSL intensity. Therefore, the following section compares the regional-averaged hourly K, K_R, K_D, and K_{RD} with ζ at 500 hPa to investigate the response relationship of K, K_R, K_D, and K_{RD} with the evolution of the ZSL intensity.

As revealed by Deng et al. (2012), Fig. 4 also shows that the variations of K, K_R, and ζ are generally synchronous, all with three obvious peaks. The peak values of K, K_R, and ζ in the three stages generally appear at 0000 LST of each day, with the maximums occurring at the vigorous stage, followed by the development stage. The minimums occur in the decay stage. The divergent kinetic energy K_D also exhibits three peaks simultaneous to when ζ has the most significant positive change at each stage of the ZSL evolution, i.e., when the ZSL develops most rapidly at each stage. The peak value of K_D is largest in the development stage, slightly smaller in the vigorous stage, and rapidly decreases in the decay stage. Note that the variation of K_D occurs roughly three hours earlier than that of ζ. One possible reason why the kinetic energy of divergent wind increases earlier than that of rotational wind is that the upper-level divergence and the low-level convergence produce ascending motion, precipitation, and consequent latent heat release, which leads to strengthened rotation. The reason for the three-hour delay may be attributed to the accuracy of the ERA5 reanalysis dataset. In addition, the evolution of K_{RD} is essentially consistent with that of ζ. However, due to the opposite signs of K_{RD} in the eastern and western parts of the ZSL (figure omitted), the hourly evolutionary characteristics of the regional-averaged K_{RD} are weaker than those of K, K_R, and K_D, as shown in Fig. 4.

In summary, the evolution of the ZSL intensity is related to K, K_R, K_D, and K_{RD}. The ZSL intensity enhances (weakens) when K, K_R, K_D, and the absolute value of K_{RD} increase (decrease), which leads to increased (decreased) precipitation. Particularly, the evolution of K and K_R are basically synchronous with the ZSL intensity, and the variation of K_D is about three hours earlier than that of the ZSL intensity.

4. Evolutionary mechanisms of the ZSL intensity

It can be seen from the above analysis that the evolution of K and K_R are basically synchronous with the ZSL intensity, and the variations in K_D occur about three hours earlier than that of the ZSL intensity. Therefore, it is reasonable to explore the evolution mechanism of the ZSL intensity by discussing the evolution of K and its components.

4.1. *Preliminary analysis of the effect of divergent and rotational winds on the kinetic energy*

The preliminary analysis of the effects of $\boldsymbol{V}_D$ and $\boldsymbol{V}_R$ on K will be discussed through the relative contributions of K_R, K_D, and K_{RD} to K,

Table 2 reveals that K, K_R, K_D, and K_{RD} increase (decrease) with the development (decay) of the ZSL, which agrees with previous conclusions. For the entire lifetime-averaged ZSL, K reaches 13.6 $\times 10^3$ J m^{-2}, where K_R makes the largest contribution, accounting for 79.1%, followed by K_D (14.9%) and the smallest by K_{RD} (only 5.9%). Noting that

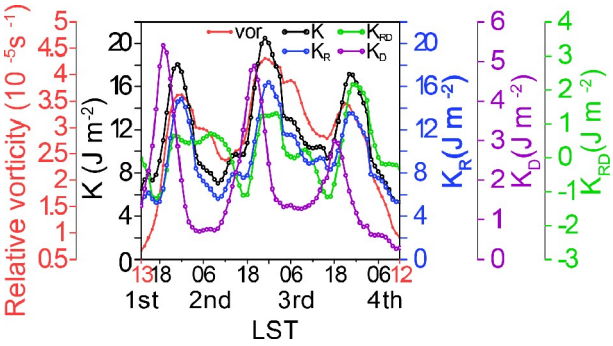

Fig. 4. Evolution of ζ (solid red lines; units: 10^{-5} s^{-1}), K (black hollow lines; units: J m^{-2}), K_R (hollow blue lines; units: J m^{-2}), K_D (hollow purple lines; units: J m^{-2}) and K_{RD} (hollow green line; units: J m^{-2}) averaged in the study area near the ZSL at 500 hPa. The black coordinate axis is for K, the purple coordinate axis for K_D, the blue coordinate axis for K_R, the green coordinate axis for K_{RD}, and the red coordinate axis for ζ.

Table 2. Area-time averaged vertical integrals of K, K_R, K_D, and K_{RD} from the surface up to 450 hPa (units: 10^3 J m^{-2}).

Period		K	K_R	K_D	K_{RD}
Development stage	Magnitude	12.099	9.247	2.149	0.703
	Percentage (%)	100	76.4	17.8	5.8
Vigorous stage	Magnitude	15.258	11.990	2.376	0.893
	Percentage (%)	100	78.6	15.6	5.8
Decay stage	Magnitude	13.532	11.123	1.577	0.832
	Percentage (%)	100	82.2	11.6	6.1
Entire lifetime	Magnitude	13.630	10.787	2.034	0.809
	Percentage (%)	100	79.1	14.9	5.9

although the relative contributions of K_R, K_D, and K_{RD} to K vary during different stages of the ZSL evolution, K_R always contributes the most (above 76%) at each stage, followed by K_D (more than 11%) and the smallest by K_{RD} (about 6%).

During the evolutionary processes of K, K_R is much larger than K_D and K_{RD}, and it contributes the most to K, accounting for about 79%, followed by K_D (about 15%) and the smallest by K_{RD} (only about 6%). Therefore, K_R plays a leading role in the evolutionary process of K, while the effects of K_D and K_{RD} are rather small.

4.2. *Influence factors of the rotational kinetic energy*

The rotational kinetic energy K_R, which contributes the most to K, is far greater than K_D and K_{RD}. Besides, the intensity evolution trend of K and K_R at 500 hPa is consistent with its evolution in the layer near the ZSL. Hence, the source of K_R at 500 hPa is investigated to reveal factors that trigger the evolution of K, with the intent of exploring the evolutionary mechanism of the ZSL intensity.

4.2.1. *Generation and transportation of the rotational kinetic energy*

At 500 hPa, the term DK_R in the development stage is only positive in the eastern part of the study area (Figs. 5a–c), and this positive-value area generally extends to the entire study area in the vigorous stage. In contrast, the entire study area is basically dominated by negative values in the decay stage. This indicates that the term K_R increases (decreases) with the strengthening (weakening) of the ZSL intensity, consistent with the results discussed above. In Figs. 5a1–c1, the term G_R is negative as the work done by the pressure gradient force consumes K_R at 500 hPa around 85°–90°E near the ZSL (figure omitted). While in the eastern and western parts near the ZSL, the pressure gradient force does positive work to produce K_R (figure omitted), which induces positive G_R (Figs. 5a1–c1). For the term HF_R, the southward V_R on the south side of the ZSL transports K to the vicinity of the ZSL (Figs. 2a–c and Figs. 4a–c), mainly causing positive HF_R near the ZSL (Figs. 5a3–a3). However, on the north side of the ZSL, the term HF_R presents an alternative distribution of positive and negative values along the latitudinal direction. Furthermore, the values of G_R and HF_R basically increase (decrease) with the enhancement (decay) of the ZSL intensity. Therefore, from the development stage to the vigorous stage of the ZSL, the term G_R in the eastern and western parts of the ZSL and the term HF_R in most areas near the ZSL are conducive to the increase of K_R, especially the K_R to the south of the ZSL. However, the terms G_R and HF_R in the abovementioned regions remain positive from the vigorous stage to the decay stage, which is not favorable for the decrease of K_R.

4.2.2. *Conversion between the divergent and rotational kinetic energies*

Figure 6 shows that the term $C(K_D, K_R)$ is positive throughout the whole lifetime of the ZSL, with a similar horizontal distribution to those of K, K_R, and K_D at 500 hPa. In addition, the values of $C(K_D, K_R)$ are significantly larger than those of G_R and HF_R (Fig. 5), basically above 4×10^{-4} W m^{-2} Pa^{-1}. This indicates a conversion from K_D to K_R throughout the whole lifetime of the ZSL, and the influence of $C(K_D, K_R)$ is more significant than those of G_R and HF_R on K_R. At the development and vigorous stages, the term $C(K_D, K_R)$ near the ZSL is positive and increases with the development of the ZSL (same as Table 3), indicating that the term $C(K_D, K_R)$ is favorable for the increase of K_R. However, the term $C(K_D, K_R)$ is still positive at the decay stage but smaller than that at the vigorous stage. In addition, the values of I_R are relatively small (figure omitted). Combined with the distributions of G_R and HF_R (Fig. 5), it can be concluded that the decrease of K_R is mainly caused by F_R (figure omitted).

As shown in Table 3, during the evolution process of the ZSL, the four terms in $C(K_D, K_R)$ are all positive, and the geostrophic effect term Af always contributes the most to $C(K_D, K_R)$. For the lifetime-averaged ZSL, the contribution rate of Af to $C(K_D, K_R)$ reaches 59.6%, followed by B (26.4%), while the contributions of Az and C are relatively smaller, being 11.3% and 2.7%, respectively. In addition, the four terms Af, Az, B, and C also increase (decrease) with the strengthening (weakening) of the ZSL intensity. Therefore, the geostrophic effect term Af among the four terms in $C(K_D, K_R)$ affects K_R the most.

4.2.3. *Geostrophic effect*

The following discussion will shed light on how Af works. The Coriolis parameter f does not change with time, so the evolution of Af is determined by the members in the term $-(v_R u_D - u_R v_D)$. It follows:

$$\mathrm{Af}(t) \propto (u_R v_D - v_R u_D)(t), \tag{9}$$

where t is time, note that $u_R v_D$ and $-v_R u_D$ have different effects on Af, as shown below.

It can be seen from Fig. 7 that the values of $u_R v_D$ (Figs. 7a1–c1) and $-v_R u_D$ (Figs. 7a2–c2) are basically positive near the ZSL, and the values of $u_R v_D$ are greater than those of $-v_R u_D$ during the entire lifetime of the ZSL. In the development stage (Fig. 7a1), there is a dense zone of the $u_R v_D$ values to the south of the study area, and the maximum $u_R v_D$ reaches 10 m^2 s^{-2}. In the vigorous stage, the values of $u_R v_D$ (Fig. 7b1) increase rapidly, with the maximum $u_R v_D$ reaching 20 m^2 s^{-2}. There is also a significant reduction of $u_R v_D$ from the vigorous stage to the decay stage, whose magnitude is less than the observed increase from the development stage to the vigorous stage (Figs. 7b1–c1). For the values of $-v_R u_D$, there is no obvious change from the development stage to the decay stage (Figs. 7a2–c2). Thus, the evolution of Af is essentially governed by the values of $u_R v_D$.

Furthermore, the values of both u_R and v_D change with the ZSL intensity evolution. Specifically, both of them increase (decrease) with the developing (decay) of the ZSL intensity (figure omitted). Therefore, the evolution of Af is

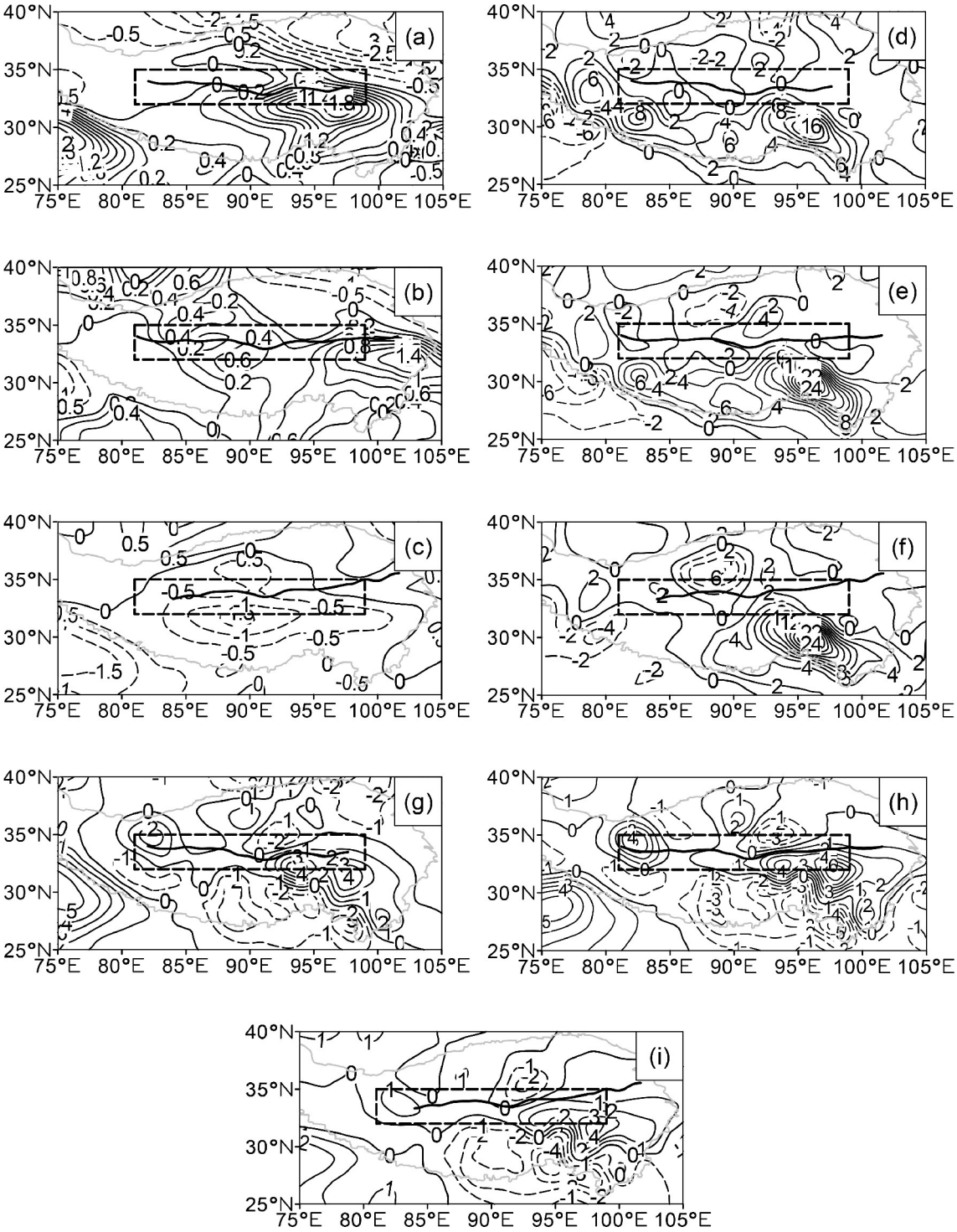

Fig. 5. Same as Fig. 3, but for (a–c) the local change of K_R (DK_R), (d–f) the generation term of K_R (G_R), and (g–i) the horizontal flux divergence of K by $\boldsymbol{V}_R$ (HF_R) (contours; units: 10^{-4} W m^{-2} Pa^{-1}).

caused by the joint actions of u_R and v_D.

The mechanism of shear line evolution is summarized as follows. In the vicinity of the ZSL, the terms of $C(K_D, K_R)$ near the ZSL, G_R in the eastern and western parts, and HF_R in most areas are all favorable factors for increasing K_R. Specifically, the term $C(K_D, K_R)$ is far larger than G_R and HF_R and thus represents the dominant factor for increasing K_R, while the decrease of K_R is mainly caused by F_R. The plausible reason for this is that energy transfer between resolvable and unresolvable scales of motion is possible because of the multi-scale ZSL in this study and that the friction near the ground is considerable because of the complex topography of the TP. Furthermore, the most important part of the conversion term is the geostrophic effect

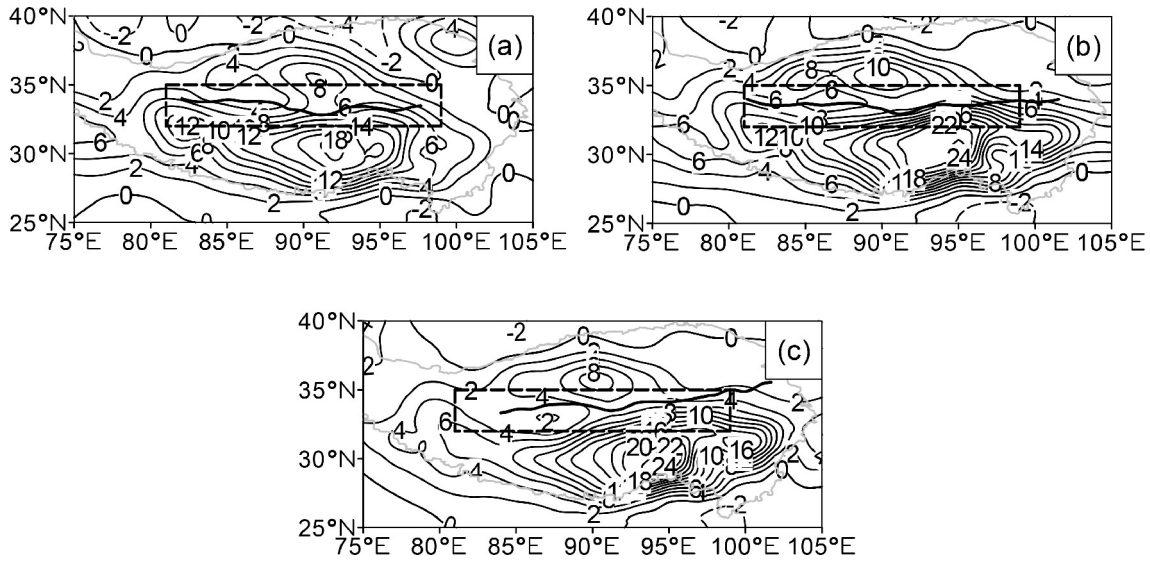

Fig. 6. Same as Fig. 3, but for conversion term between K_D and K_R (C(K_D, K_R)) (contours; units: 10^{-4} W m^{-2} Pa^{-1}).

Table 3. Same as Table 2, but for $C(K_D, K_R)$ (units: 10^3 J m^{-2}).

Period		$C(K_D, K_R)$	Af	Az	B	C
Development stage	Magnitude	0.546	0.330	0.059	0.143	0.014
	Percentage (%)	100	60.4	10.8	26.2	2.6
Vigorous stage	Magnitude	0.798	0.474	0.1	0.201	0.022
	Percentage (%)	100	59.4	12.5	25.2	2.8
Decay stage	Magnitude	0.535	0.314	0.055	0.15	0.016
	Percentage (%)	100	58.7	10.3	28	3
Entire lifetime	Magnitude	0.626	0.373	0.071	0.165	0.017
	Percentage (%)	100	59.6	11.3	26.4	2.7

term Af, and the joint action of u_R and v_D determines the evolution of Af**.**

5. Conclusions and discussion

By using the ERA5 reanalysis dataset and the daily precipitation data from the daily meteorological dataset of basic meteorological elements of China National Surface Weather Station (version 3.0) from June to August during 1980–2019, 11 cases of ZSLs that cause heavy precipitation and have a lifetime of more than 60 hours in a high-frequency region for ZSL occurrence (32°–35°N) are selected for composite analysis. By decomposing K into the terms of K_D, K_R, and K_{RD}, the relationship of K_D, K_R, and K_{RD} with the evolution of the ZSL intensity is investigated. In addition, the evolution mechanisms of the ZSL intensity are also preliminarily explored from the perspective of K_D and K_R. The main conclusions are as follows.

(1) There are cyclonic $\boldsymbol{V}_R$ and convergent $\boldsymbol{V}_D$ near the ZSL, and the magnitude of $\boldsymbol{V}_R$ is generally larger than that of $\boldsymbol{V}_D$.

(2) The ZSL intensity evolution is basically synchronous with that of K, $K_{R.,}$ and K_{RD} but lags behind that of K_D by about three hours. Therefore, the precipitation caused by ZSLs could be predicted by monitoring the evolution of K_D.

(3) During the processes of the ZSL intensity evolution, K_R contributes the most to K, accounting for about 79%, while the effects of K_D and K_{RD} to K are rather small.

(4) The rotational kinetic energy budget shows that the increase in K_R is governed by the conversion from K_D to K_R. Furthermore, the most important part of the conversion term is the geostrophic effect term Af, and the evolution of Af is determined by the joint action of the zonal rotational and meridional divergent wind components. Therefore, the enhancement of the ZSL intensity is mainly controlled by the joint increase of the zonal rotational and meridional divergent wind components. In contrast, the attenuation of the ZSL intensity is primarily attributed to friction and transfers of energy between resolvable and unresolvable scales of motion.

In this research, from a large sample of ZSLs over the TP during a long summertime period, 11 typical cases of ZSLs that cause heavy precipitation and maintain for a long time are systematically selected for composite analysis, aiming to overcome the limitations in analysis with individual case and thus get more representative results. From the per-

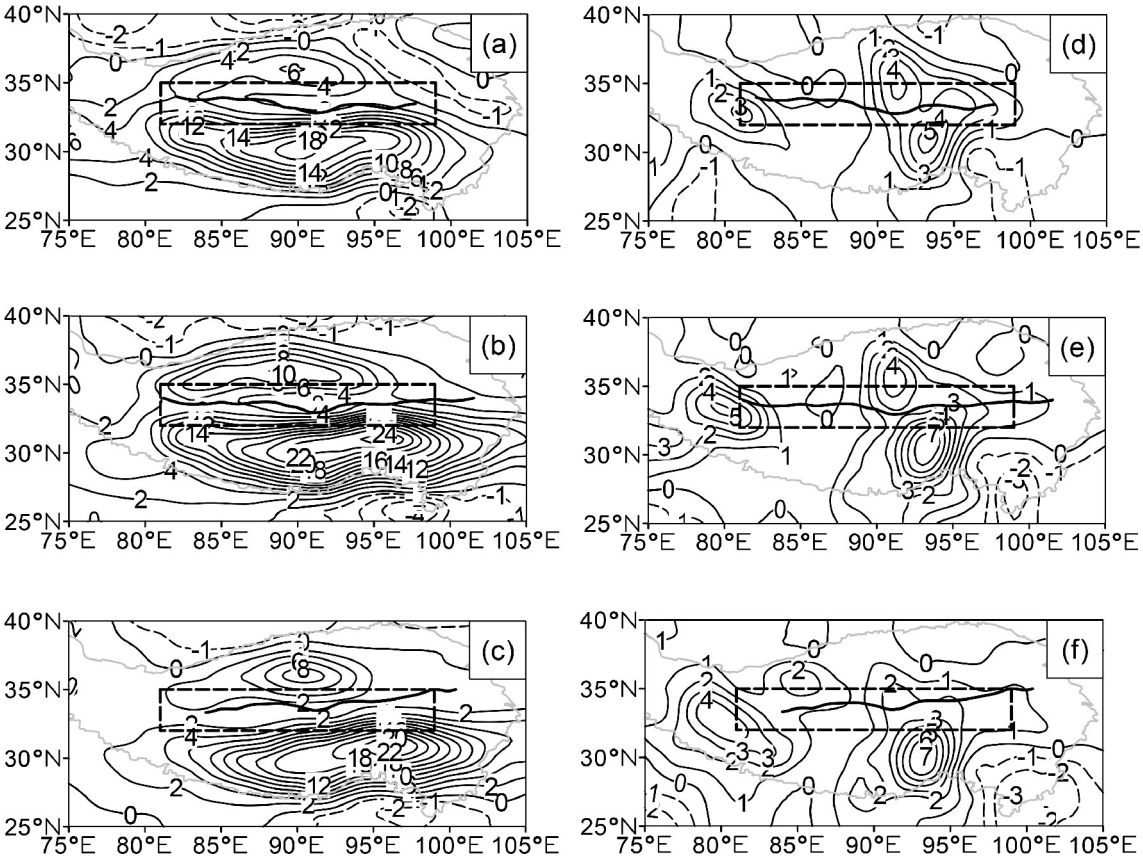

Fig. 7. (a1–c1) Same as Fig. 3, but for (a1–c1). The values of times zonal rotational wind component times meridional divergent wind component ($u_R v_D$) and (a2–b2) the opposite values of zonal divergent wind component times meridional rotational wind component ($-v_R u_D$) are shown (contours; units: $m^2\ s^{-2}$).

spective of the divergent and rotational kinetic energies (K_D and K_R), the relationship of K_D and K_R with the evolution of the ZSL intensity is obtained, which further improves the understanding of the ZSL evolution. In addition, during the evolutionary process of ZSLs, the source of K_D and the kinetic energy balance between K_R and K_D require further study. It should be noted that the results in this study are based on the composite analysis of 11 cases of ZSLs of a specific type, and the evolutionary mechanisms of other types of zonal shear lines over the TP need to be further explored.

Acknowledgements. The authors thank Jiali MA and Qiaohua LIU for their help with this study. This work was supported by the Key Program of the National Science Foundation of China (Grant No. 42030611), the Second Tibetan Plateau Scientific Expedition and Research (STEP) program (Grant No. 2019QZKK0105), the Integration Project of Major Research Program of the National Natural Science Foundation of China (Grant No. 91937301), the General Program of the National Science Foundation of China (Grant No. 42175008).

REFERENCES

Bolin, B., 1950: On the influence of the Earth's orography on the general character of the westerlies. *Tellus*, **2**(3), 184–195, https://doi.org/10.3402/tellusa.v2i3.8547.

Buechler, D. E., and H. E. Fuelberg, 1986: Budgets of divergent and rotational kinetic energy during two periods of intense convection. *Mon. Wea. Rev.*, **114**(1), 95–114, https://doi.org/10.1175/1520-0493(1986)114<0095:BODARK>2.0.CO;2.

Chen, J., and G. P. Li, 2018: Diagnosis analysis on a plateau shear line process based on NASA MERRA reanalysis datasets. *Scientia Meteorologica Sinica*, **38**(3), 320–330, https://doi.org/10.3969/2017jms.0073. (in Chinese with English abstract)

Chen, T. C., J. D. Alpert, and T. W. Schlatter, 1978: The effects of divergent and nondivergent winds on the kinetic energy budget of a mid-latitude cyclone: A case study. *Mon. Wea.*

Rev., **106**(4), 458–468, https://doi.org/10.1175/1520-0493(1978)106<0458:TEODAN>2.0.CO;2.

Deng, D. F., Y. S. Zhou, and D. H. Wang, 2012: The application of wind and water-vapor flux partitioning technique to the structure of a northeast vortex in 2006. *Chinese Journal of Geophysics*, **55**(6): 1852–1866, 10.6038/j.issn.0001-5733.2012.06.006. (in Chinese with English abstract)

Ding, Y. H., and Y. Z. Liu, 1986: Study on the kinetic energy budget of a Typhoon—budgets of kinetic energy in general flow and eddy kinetic energy. *Science in China Series B*, **29**(2), 187–200.

Endlich, R. M., 1967: An iterative method for altering the kinematic properties of wind fields. *J. Appl. Meteor. Climatol.*, **6**(5), 837–844, https://doi.org/10.1175/1520-0450(1967)006<0837:AIMFAT>2.0.CO;2.

Flohn, H., 1957: Large-scale aspects of the "summer monsoon" in South and East Asia. *J. Meteor. Soc. Japan*, **35A**, 180–186, https://doi.org/10.2151/jmsj1923.35A.0_180.

Fu, S. M., J. H. Sun, S. X. Zhao, and W. L. Li, 2011: The energy budget of a southwest vortex with heavy rainfall over South China. *Adv. Atmos. Sci.*, **28**(3), 709–724, https://doi.org/10.1007/s00376-010-0026-z.

Fu, S. M., F. Yu, D. H. Wang, and R. D. Xia, 2013: A comparison of two kinds of eastward-moving mesoscale vortices during the mei-yu period of 2010. *Science China Earth Sciences*, **56**(2): 282–300, https://doi.org/10.1007/s11430-012-4420-5.

Fuelberg, H. E., and P. A. Browning, 1983: Roles of divergent and rotational winds in the kinetic energy balance intense convective activity. *Mon. Wea. Rev.*, **111**(11), 2176–2193, https://doi.org/10.1175/1520-0493(1983)111<2176:RODARW>2.0.CO;2.

Hawkins, H. F., and S. L. Rosenthal, 1965: On the computation of stream functions from the wind field. *Mon. Wea. Rev.*, **93**(4), 245–252, https://doi.org/10.1175/1520-0493(1965)093<0245:OTCOSF>2.3.CO;2.

He, G. B., W. L. Gao, and N. N. Tu, 2009: The observational analysis of shear line and low vortex over the Tibetan Plateau in summer from 2000 to 2007. *Plateau Meteorology*, **28**(3): 549–555. (in Chinese with English abstract)

Jin, S. L., S. L. Feng, W. Shen, S. M. Fu, L. Z. Jiang, and J. H. Sun, 2020: Energetics characteristics accounting for the low-level wind's rapid enhancement associated with an extreme explosive extratropical cyclone over the western North Pacific Ocean. *Atmos. Ocean. Sci. Lett.*, **13**(5), 426–435, https://doi.org/10.1080/16742834.2020.1763153.

Li, W. L., R. D. Xia, J. H. Sun, S. M. Fu, L. Z. Jiang, B. F. Chen, and F. Y. Tian, 2019: Layer-wise formation mechanisms of an entire-troposphere-thick extratropical cyclone that induces a record-breaking catastrophic rainstorm in Beijing. *J. Geophys. Res. Atmos.*, **124**(20): 10 567–10 591, https://doi.org/10.1029/2019JD030868.

Luo, X., and G. P. Li, 2019a: Eddy kinetic energy characteristics of an eastward plateau shear line. *Journal of the Meteorological Sciences*, **39**(2), 226–236, https://doi.org/10.3969/2018jms.0067. (in Chinese with English abstract)

Luo, X., and G. P. Li, 2019b: The decomposition of kinetic energy based on spatial scale and its application in the process of the plateau shear line. *Plateau Meteorology*, **38**(2), 314–324, https://doi.org/10.7522/j.issn.1000-0534.2018.00106. (in Chinese with English abstract)

Ma, J. L., and X. P. Yao, 2015: Statistical analysis of the shear lines and torrential rains over the Yangtze-Huaihe river region during June-July in 1981–2013. *Acta Meteorologica Sinica*, **73**(5): 883–894, https://doi.org/10.11676/qxxb2015.065.

Pearce, R. P., 1974: The design and interpretation of diagnostic studies of synoptic-scale atmospheric systems. *Quart. J. Roy. Meteor. Soc.*, **100**(425), 265–285, https://doi.org/10.1002/qj.49710042502.

Shi, R., and G. B. He, 2011: Contrast analysis on background circulation of plateau shear line moving out and not moving out of the Tibetan Plateau. *Plateau Meteorology*, **30**(6): 1453–1461. (in Chinese with English abstract)

Tang H., 2002: Analysis of heavy precipitation process over Xizang Plateau in Summer. *Tibet's Cience and Technology*, **2**(9): 51–55. (in Chinese)

Tao, S. Y., 1980: *Heavy Rainfalls in China*. Science Press, 225pp. (in Chinese)

Tao, S. Y., S. W. Luo, and H. C. Zhang, 1984: The Qinghai-Xizang Plateau meteorological science experiment and its observation system from May to August. *Meteor. Mon.*, **10**(7), 2–5, https://doi.org/10.7519/j.issn.1000-0526.1984.7.001. (in Chinese)

The Tibetan Plateau Science Research Group, 1981: *Vortex Shear Line Study at 500 hPa over the Tibetan Plateau in Summer*. Science Press, 122pp. (in Chinese)

Tu, N. N., and G. B. He, 2010: Case analysis on two low vortexes induced by Tibetan Plateau shear line. *Plateau Meteorology*, **29**(1): 90–98. (in Chinese with English abstract)

Wu, G. X., J. Y. Mao, A. M. Duan, and Q. Zhang, 2004: Recent progress in the study on the impacts of Tibetan Plateau on Asian summer climate. *Acta Meteorologica Sinica*, **62**(5), 528–540, https://doi.org/10.3321/j.issn:0577-6619.2004.05.002. (in Chinese with English abstract)

Yao, X. P., X. Zhang, and J. L. Ma, 2020: Characteristics of the meridionally oriented shear lines over the Tibetan Plateau and its relationship with rainstorms in the boreal summer half-year. *Journal of Tropical Meteorology*, **26**(1), 93–102, https://doi.org/10.16555/j.1006-8775.2020.009.

Ye, D. Z., 1981: Some characteristics of the summer circulation over the Qinghai-Xizang (Tibet) Plateau and its neighborhood. *Bull. Amer. Meteor. Soc.*, **62**(1), 14–19, https://doi.org/10.1175/1520-0477(1981)062<0014:SCOTSC>2.0.CO;2.

Ye, D. Z., and Y. X. Gao, 1979: *Qinghai-Xizang Plateau Meteorology*. Science Press, 122–126. (in Chinese)

Yu, S. H., 1994: A *Q*-vector analysis of the process of shear lines on Qinghai–Xizang Plateau triggered from moving Trough aloft. *Quarterly Journal of Applied Meteorology*, **5**(1): 109–113. (in Chinese with English abstract)

Yu, S. H., and H. Luo, 1993: The contrast analysis of kinetic energy budget for developing trough and shear line over the Qinghai-Xizang Plateau. *Plateau Meteorology*, **12**(3): 251–256. (in Chinese with English abstract)

Yu, Y. B., and X. P. Yao, 1999a: Divergent and Rotational wind kinetic energy budget and conversion during a torrential rain process caused by Typhoon low pressure trough. *Acta Meteorologica Sinica*, **57**(4), 439–449, https://doi.org/10.11676/qxxb1999.041. (in Chinese with English abstract)

Yu, Y. B., and X. P. Yao, 1999b: The energetic analysis of the typhoon low pressure and its torrential rain in summer north China. *Journal of Tropical Meteorology*, **15**(2): 177–185. (in Chinese with English abstract)

Zhang, S., X. P. Yao, and Y. F. Gong, 2019: A synthetic study of the structure and evolution characteristics of a meridionally-oriented Shearline over the Tibetan Plateau based on objective identification. *Acta Meteorologica Sinica*, **77**(6), 1086–1106, https://doi.org/10.11676/qxxb2019.058. (in Chinese with English abstract)

Zhang, X., X. P. Yao, J. L. Ma, and Z. G. Mima, 2016: Climatology of transverse shear lines related to heavy rainfall over the Tibetan Plateau during boreal summer. *J. Meteor. Res.*, **30**(6), 915–926, https://doi.org/10.1007/s13351-016-6952-7.

Zhao, D. J., and X. P. Yao, 2018: Case study on shape evolution of plateau shear line: Structural characteristics. *Plateau Meteorology*, **37**(2), 420–431, https://doi.org/10.7522/j.issn.1000-0534.2017.00066. (in Chinese with English abstract)

Zhao, D. J., W. J. Zhu, Y. B. Yu, and X. P. Yao, 2009: Analysis of kinetic energy feature of abrupt intensity change of super Typhoon Saomai (0608). *Journal of Tropical Meteorology*, **25**(2), 141–146, https://doi.org/10.3969/j.issn.1004-4965.2009.02.002. (in Chinese with English abstract)

Zhou, Y. S., D. F. Deng, and J. T. Li, 2014: Rainstorm amplification of Typhoon Bilis (0604) and its wind structural change. *Chinese Journal of Atmospheric Sciences*, **38**(3), 563–576, https://doi.org/10.3878/j.issn.1006-9895.2013.12220. (in Chinese with English abstract)